Pressure-induced organic topological nodal-line semimetal in the three-dimensional molecular crystal $Pd(dddt)_2$

Zhao Liu,[1] Haidi Wang,[1] Z. F. Wang,[1,2,*] Jinlong Yang,[1,3,†] and Feng Liu[4,5,‡]

[1]*Hefei National Laboratory for Physical Sciences at the Microscale, University of Science and Technology of China, Hefei, Anhui 230026, China*

[2]*CAS Key Laboratory of Strongly-Coupled Quantum Matter Physics, University of Science and Technology of China, Hefei, Anhui 230026, China*

[3]*Synergetic Innovation Center of Quantum Information and Quantum Physics, University of Science and Technology of China, Hefei, Anhui 230026, China*

[4]*Department of Materials Science and Engineering, University of Utah, Salt Lake City, Utah 84112, USA*

[5]*Collaborative Innovation Center of Quantum Matter, Beijing 100084, China*

(Received 18 September 2017; published 18 April 2018)

The nodal-line semimetal represents a class of topological materials characterized with highest band degeneracy. It is usually found in inorganic materials of high crystal symmetry or a minimum symmetry of inversion aided with accidental band degeneracy [Phys. Rev. Lett. **118**, 176402 (2017)]. Based on first-principles band structure, Wannier charge center, and topological surface state calculations, here we predict a pressure-induced topological nodal-line semimetal in the absence of spin-orbit coupling (SOC) in the synthesized single-component 3D molecular crystal $Pd(dddt)_2$. We show a Γ-centered single nodal line undulating within a narrow energy window across the Fermi level. This intriguing nodal line is generated by pressure-induced accidental band degeneracy, without protection from any crystal symmetry. When SOC is included, the fourfold degenerated nodal line is gapped and $Pd(dddt)_2$ becomes a strong 3D topological metal with an Z_2 index of (1;000). However, the tiny SOC gap makes it still possible to detect the nodal-line properties experimentally. Our findings afford an attractive route for designing and realizing topological states in 3D molecular crystals, as they are weakly bonded through van der Waals forces with a low crystal symmetry so that their electronic structures can be easily tuned by pressure.

DOI: 10.1103/PhysRevB.97.155138

The development of topological theory in condensed matter physics opens up a field of topological materials exhibiting exotic quantum phases. Topological materials are usually characterized with symmetry-protected highly degenerated bands. For example, among topological semimetals (TSMs), the Dirac [1–4] and Weyl [5–9] semimetal is characterized by fourfold and twofold discrete band degenerate points, respectively, while the nodal-line semimetal [10–16] is characterized by the fourfold continuous band degenerate lines. The crystal symmetry plays an important role in generating the TSM states, in particular, the nodal-line semimetals are usually predicted in high-symmetry crystals with mirror symmetry [16]. The nodal lines are constrained in the mirror planes in momentum space, and vanish upon breaking of mirror symmetry. Such a high-symmetry requirement greatly limits the material prediction for nodal-line semimetals. Very interestingly, Quan *et al.* has recently demonstrated that a minimum symmetry of inversion can sufficiently induce a nodal line by accidental band degeneracy [14]. This finding makes it possible to search nodal lines in low-symmetry materials that are largely overlooked in previous studies, since the nodal lines may appear via accidental band degeneracy at arbitrary k points in momentum space. However, it is unclear how general this mechanism can work and, better yet, whether one can generate such accidental band degeneracy by external field effects to realize the nodal-line semimetal in a controllable manner.

Strain engineering has been proven a powerful approach in tuning the band structures of conventional semiconductors [17] as well as contemporary low-dimensional quantum materials [18], which can be naturally expected to offer an attractive route to controllably tuning "bands" of topologically materials. Both band gap and band degeneracy can be effectively altered by applying strain or pressure. Intuitively, the band gap of a topological insulator may be closed by applying isotropic compressive strain (or hydrostatic pressure) while band degeneracy may be lifted by applying anisotropic (uniaxial/biaxial) strain to lower the crystal symmetry; both can induce a topological phase transition. Less intuitively, it has been recently shown that spin transport properties of a quantum spin Hall insulator can be drastically modified by applying a bending strain [19,20]. In this paper, we demonstrate a form of strain engineering approach in which pressure not just closes the band gap of a semiconductor but also causes a high degree of accidental band degeneracy to induce a topological phase transition forming a nodal-line semimetal in a 3D molecular crystal with low symmetry.

Generally, organic materials have a lower crystal symmetry than inorganic materials, so they are less likely to satisfy the high-symmetry requirement for realizing nodal-line semimet-

*zfwang15@ustc.edu.cn
†jlyang@ustc.edu.cn
‡fliu@eng.utah.edu

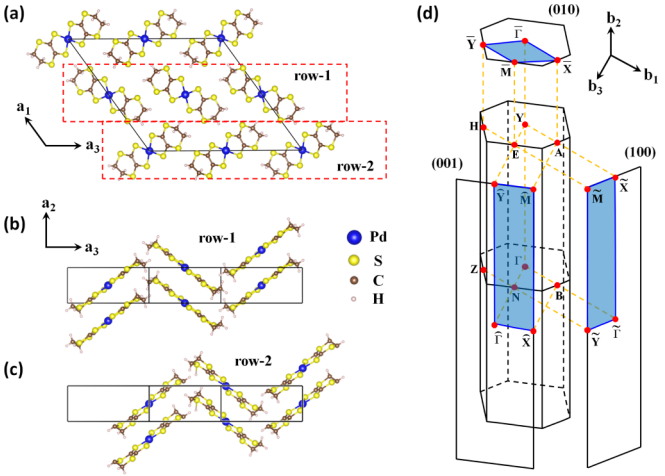

FIG. 1. (a) Top view of the 3D molecular crystal of $Pd(dddt)_2$ at ambient pressure. The dashed rectangle denotes two independent molecular rows, labeled as row-1 and row-2. (b) and (c) Side views of row-1 and row-2, respectively. (d) Bulk BZ and three projected surface BZs of (100), (010), and (001) surfaces.

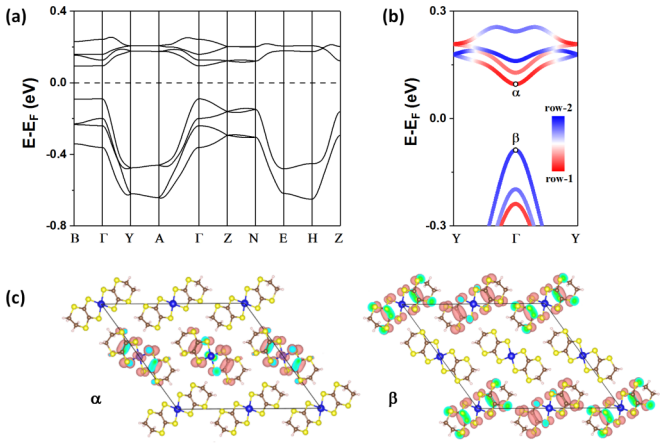

FIG. 2. (a) Band structure of $Pd(dddt)_2$ without SOC at ambient pressure. (b) Layer projected band structure along Γ-Y direction around the Fermi level in (a). (c) Partial charge density distribution at two chosen k points (α and β) labeled in (b).

als. Surprisingly, we discover a pressure-induced topological nodal-line semimetal in the synthesized single-component 3D molecular crystal $Pd(dddt)_2$ (dddt = 5,6-dihydro-1,4-dithiin-2,3-dithiolate). Based on first-principles calculations, we identify a Γ-centered nodal line when SOC is neglected. Physically, the nodal line around the Fermi level is generated by the pressure-induced accidental band degeneracy between states of two real-space-separated stacking molecular rows, which can be described by a two-band $k \cdot p$ Hamiltonian. Its nontrivial band topology is directly identified by both Wannier charge center evolution and drumheadlike surface state. The topological nodal line is not protected by any crystal symmetry, and is gapped by including SOC to become a strong 3D topological metal, as confirmed by both Z_2 index and topological surface-state calculations. Our results demonstrate the possibility of controllably generating 3D topological states by pressure, and pave the way for searching and designing topological states in 3D organometallic materials [21–26] by strain engineering.

Our first-principles calculations are carried out in the framework of generalized gradient approximation with Perdew-Burke-Ernzerhof functionals using the Vienna *Ab initio* Simulation Package (VASP) [27]. All the calculations are performed with a plane-wave cutoff of 500 eV on the $4 \times 16 \times 4$ Monkhorst-Pack k-point mesh, and the convergence criterion of energy is 10^{-5} eV. During the structural relaxation, all atoms are relaxed until the forces are smaller than 0.01 eV·Å^{-1}.

The crystal structure of $Pd(dddt)_2$ (space group $P\frac{2_1}{c}$) at ambient pressure is shown in Fig. 1(a). The molecular crystal is made of four $Pd(dddt)_2$ molecules per unit cell, which constitutes one molecular layer, and such layers are stacked face-to-face through the van der Waals interaction without forming any chemical bonds between the layers, as shown in Figs. 1(b) and 1(c). Within each layer, four $Pd(dddt)_2$ molecules can be further divided into two stacking rows, labeled as row-1 and row-2 in Fig. 1(a). Each row has two $Pd(dddt)_2$ molecules, which are related by the screw rotation $\{C_{2y}|0\frac{1}{2}\frac{1}{2}\}$ (y axis is along a_2). Figure 1(d) shows the bulk and three surface projected Brillouin zones (BZs) with high symmetric k points. The band structure of $Pd(dddt)_2$ without SOC at ambient pressure is shown in Fig. 2(a). It shows a semiconductor with a Γ-point gap of ∼184 meV. The band components around the Γ point are shown in Fig. 2(b). We particularly note that the valence and conduction band is constituted from molecular orbitals residing in row-2 and row-1, respectively, which are separated in real space. The row-separated states can be seen clearly from the real-space distribution of partial charge density at two chosen k points (α and β at Γ point), as shown in Fig. 2(c). The α and β state belongs to the 1D irreducible representation of little co-group C_{2h} at Γ point, namely, α and β state belongs to B_g and A_u, respectively.

Recently, Kato *et al.* has reported a transport experiment for the single-component 3D molecular crystal of $Pd(dddt)_2$ under hydrostatic pressure [28]. They found that the resistivity of $Pd(dddt)_2$ decreases continuously with the increasing pressure, showing a pressure-induced band-gap reduction. Interestingly, a temperature-independent resistivity is observed above a critical pressure, indicating the emergence of the Dirac state in $Pd(dddt)_2$ under pressure. Next, we calculate the band structure of $Pd(dddt)_2$ without SOC at 8 GPa pressure, which has also been reported by Kato *et al.* [28]. Here, the pressure does not change the space group of $Pd(dddt)_2$, but shrinks only the lattice constants (see Table I). As shown in Fig. 3(a), the semiconductor gap is closed and a pair of Dirac points seemed to appear along Γ-Y direction, siting at the fractional coordinate of (0.0, ±0.09, 0.0) in momentum space. So at the first sight, one might think the pressured $Pd(dddt)_2$ is a 3D

TABLE I. Lattice parameter of $Pd(dddt)_2$ crystal.

Pressure	a_1	a_2	a_3	α	β	γ
0 GPa	18.46 Å	4.73 Å	20.43 Å	90°	125.65°	90°
8 GPa	17.24 Å	4.25 Å	19.44 Å	90°	126.27°	90°

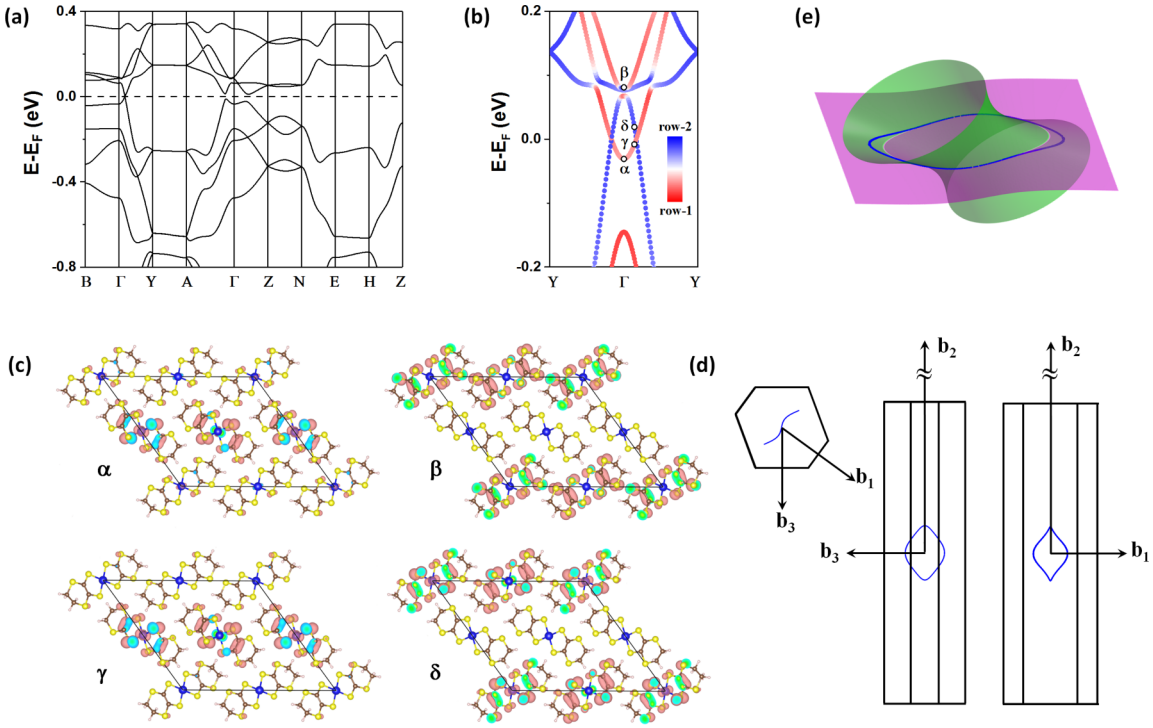

FIG. 3. (a) Band structure of $Pd(dddt)_2$ without SOC at 8 GPa pressure. (b) Layer projected band structure along Γ-Y direction around the Fermi level in (a). (c) Partial charge-density distribution at four chosen k points (α, β, γ, and δ) labeled in (b). (d) Top and side views of the pressure-induced 3D nodal line (solid blue line) in the bulk BZ. (e) Comparison of the nodal line obtained from $k \cdot p$ (the intersection of two colored surfaces) and first-principles calculations (solid blue line). The corresponding fitting parameters are $a_0 = 0.024$, $a_1 = 0.412$, $a_2 = 2.921$, $a_3 = 1.756$, $b_1 = 0.089$, $b_3 = 0.084$, $d_1 = 0.238$, $d_3 = 2.087$, $c_0 = 0.032$, $c_1 = 0.223$, $c_2 = 4.030$, and $c_3 = 1.360$.

Dirac semimetal. However, this assignment turns out to be incorrect.

To have a better understanding about the pressured electronic structure of $Pd(dddt)_2$, we have further checked its band components around the Dirac point, as shown in Fig. 3(b). The valence and conduction band at the Fermi level is still constituted from molecular orbitals of different rows. However, under pressure, the spacing between row-1 and row-2 becomes smaller, causing further interaction between their associated electronic states, i.e., the valence and conduction band-edge states overlap and close the band gap. The real-space distribution of partial charge density at four chosen k points, two at Γ point (α and β) and two near Dirac points (γ and δ), are shown in Fig. 3(c). Now, these states become overlapped in momentum and energy space but remain "separated" in real space (the row-1 and row-2 are not related by the lattice symmetry). One also notes that pressure has a rigid effect on the band structure, namely, it inverts α and β state without changing their irreducible representations, so the distribution of partial charge densities resemble those at ambient pressure. The two crossed bands in Fig. 3(b) belong to different irreducible representations of point C_2, which is the little co-group of high symmetry line Γ-Y. Therefore, the Dirac point is exactly gapless at $(0.0, \pm 0.09, 0.0)$. Additionally, previous theoretical works have already shown that in the case of coexistence of space inversion and time reversal symmetry, the two crossed bands with gapless points will cross along a closed nodal line rather than isolated Dirac points [9,10]. Here, the molecular crystal of $Pd(dddt)_2$ under pressure satisfies all these conditions. Therefore, the Dirac point along Γ-Y direction in Fig. 3(b) is, as a matter of fact, just one degenerate point along the entire nodal line and the pressured $Pd(dddt)_2$ should be classified as a 3D nodal-line semimetal instead of a 3D Dirac semimetal in the absence of SOC.

To further elaborate on the above statement, we have fitted an eight-band first-principles tight-binding (TB) Hamiltonian of $Pd(dddt)_2$ without SOC by using the maximally localized Wannier functions in WANNIER90 package [29]. Using this TB Hamiltonian, the bulk band degeneracy around the Fermi level within the BZ is calculated using a very dense k-point mesh. As expected, a Γ-centered single 3D nodal line can be mapped out, as shown in Fig. 3(d). From the top and side views of Fig. 3(d), one can see the nodal line has a snakelike shape, with space inversion (P), mirror (M_y), and rotation (C_{2y}) symmetry. In our calculation, the band degeneracy is defined by the bulk gap smaller than 0.5 meV. This value will decrease with the increasing k-point mesh, but the overall nodal-line shape is not changed. In addition, we find that the nodal-line energy is not exactly at the Fermi level, but lies within a very narrow energy window from −7 to 7 meV, illustrating a flat nodal line in energy space.

The Γ-centered nodal line can also be described by a simple two-band $k \cdot p$ Hamiltonian. The general two-band nodal-line Hamiltonian can be written as [10]

$$H(\mathbf{k}) = \sum_{i=0}^{3} g_i(\mathbf{k})\sigma_i, \tag{1}$$

where $g_i(\mathbf{k})$ are real functions of $\mathbf{k}$, σ_0 is the identity matrix, and σ_i is the Pauli matrix for the space expanded by α and β state near the Fermi level. Thus, the space inversion (P) and time reversal (T) symmetry can be written as $P = \sigma_z$ and $T = \sigma_z K$ (we choose $T = PK$ to make the Hamiltonian real, and K is the complex conjugate operator as usual), respectively. The coexistence of space inversion and time-reversal symmetry leads to $g_2 = 0$, g_0, g_1, and g_3 being even, odd and even functions of $\boldsymbol{k}$, respectively [10]. Thus, by considering the crystal symmetry at Γ point and up to the third order of $\boldsymbol{k}$, $g_i(\mathbf{k})$ are given as

$$\begin{aligned} g_0(\mathbf{k}) &= a_0 + a_1k_1^2 + a_2k_2^2 + a_3k_3^2, \\ g_1(\mathbf{k}) &= b_1k_1 + b_3k_3 + d_1k_1^3 + d_3k_3^3, \\ g_2(\mathbf{k}) &= 0, \\ g_3(\mathbf{k}) &= c_0 + c_1k_1^2 + c_2k_2^2 + c_3k_3^2. \end{aligned} \tag{2}$$

Here, $g_0(\mathbf{k})$ controls the nodal-line energy, and $g_1(\mathbf{k}) = g_3(\mathbf{k}) = 0$ controls the nodal-line shape in momentum space. As shown in Fig. 3(e), the $k \cdot p$ nodal line (the intersection of two colored surfaces, which is flat for $g_1(\mathbf{k}) = 0$ and hyperboloid for $g_3(\mathbf{k}) = 0$) shows very good agreement with the first-principles nodal line (solid blue line).

For a spinless system with both space inversion and time reversal symmetry, the Berry phase can be either 0 or π, evolving on an arbitrary closed loop in the BZ. Equivalently, the total 1D hybrid Wannier charge center (WCC) [$z(k_x,k_y) = \sum_n z_n(k_x,k_y)$, the summation over the Wannier charge centers (z_n) of all the occupied bands (n is band index)] [30–32] will have a quantized value of either 0 or 0.5. When passing through the projected nodal line in the k_x-k_y plane, a value jump between 0 and 0.5 will be observed [12], signifying a topological nodal line. To demonstrate this point, the total WCC of the pressured Pd(dddt)$_2$ is calculated along Y-Γ-Y direction in the (001) surface BZ [dashed red line in the inset BZ in Fig. 4(a)]. As shown in Fig. 4(a), the value of total WCC is indeed 0.5 and 0 inside and outside the projected nodal line, respectively, as expected.

In addition, due to the bulk-boundary correspondence, another signature of the topological nodal line is the existence of a drumheadlike surface state [10,15]. To identify this signature, using the TB Hamiltonian incorporated with the recursive surface Green's function method [25], the semi-infinite surface state on (001) surface is calculated. As shown in Fig. 4(b), there is one topological surface state inside the nodal line, and two trivial dangling-bond surface states outside the nodal line. One can see that two gapless Dirac points, the projected nodal points along Y-Γ-Y direction, are connected by the topological surface state. Furthermore, two constant energy contours of (001) surface around the Γ point with chemical potential (μ) of −3 meV and −5 meV are shown in Figs. 4(c) and 4(d), respectively. Clearly, the topological surface state is nestled in the interior of the projected nodal line on (001) surface, and has a drumheadlike shape. Therefore, both the nonzero total WCC and the drumheadlike surface state confirm the topological nodal-line semimetal phase in Pd(dddt)$_2$.

It is worth noting that a single nodal line can serve as the basic building block of complicated nodal-line structures. In this regard, our finding provides an ideal organic platform to investigate the nodal-line-related physics, such as anisotropic Friedel oscillation [33], large intrinsic spin Hall effect [34], 3D quantum Hall effect [35], and strong correlation effect [36]. In turn, these studies may help advance our fundamental understanding of the intriguing physical phenomena in other topological materials with complicated nodal-line structures. Moreover, we also find that the pressure-induced nodal line in Pd(dddt)$_2$ is robust to a finite perturbation of the pressure. Therefore, it is different from the fine-tuning lattice parameters induced topological phase at the critical point.

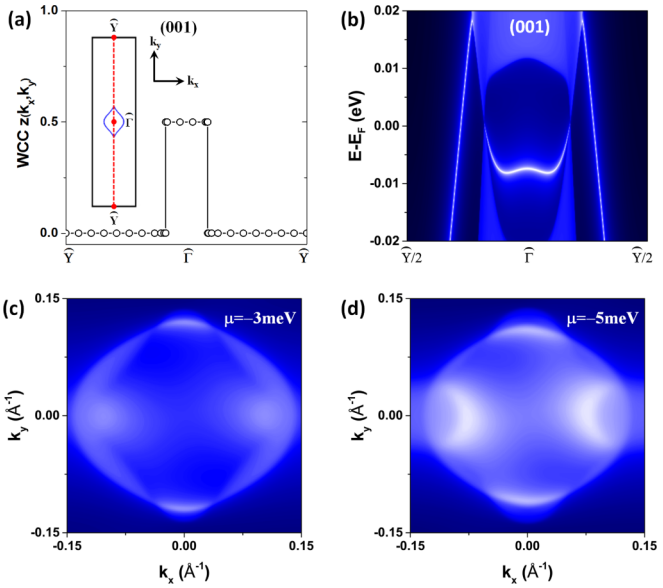

FIG. 4. (a) Evolution of total WCC along high symmetric direction in the (001) surface BZ. The inset is (001) surface BZ with a high symmetric k point and the projected nodal line (solid blue line). (b) Topological surface state on (001) surface without SOC. (c) and (d) 2D constant energy contours of (001) surface around the Γ point with chemical potential of −3 meV and −5 meV, respectively.

After confirming the topological nodal-line semimetal phase in the pressured Pd(dddt)$_2$, next we consider the effect of SOC on its electronic structures. As shown in Fig. 5(a), the overall band structure with SOC is the same as that without SOC [Fig. 3(a)]. Zoom in on the band around the band degenerate point at Fermi level along the Γ-Y direction and a small SOC gap of ∼3 meV is observed, as shown in Fig. 5(b). The α and β states at Γ point have the same eigenvalue under the mirror symmetry (M_y). Thus, by including SOC, the nodal line will be hybridized and an SOC gap is opened along the entire nodal line [37]. To support the above symmetry analysis, the band degeneracy along the nodal line is checked again using the same criterion as in the case without SOC. We found that the SOC completely lifts the degeneracy of the entire nodal line. Although the nodal-line energy has a relatively narrow distribution, nevertheless the weak SOC in Pd(dddt)$_2$ cannot override the band dispersion to open a global gap along the nodal line. Consequently, the SOC only opens a local gap along the nodal line in the BZ. Additionally, the SOC gap size is less sensitive to pressure and calculation method.

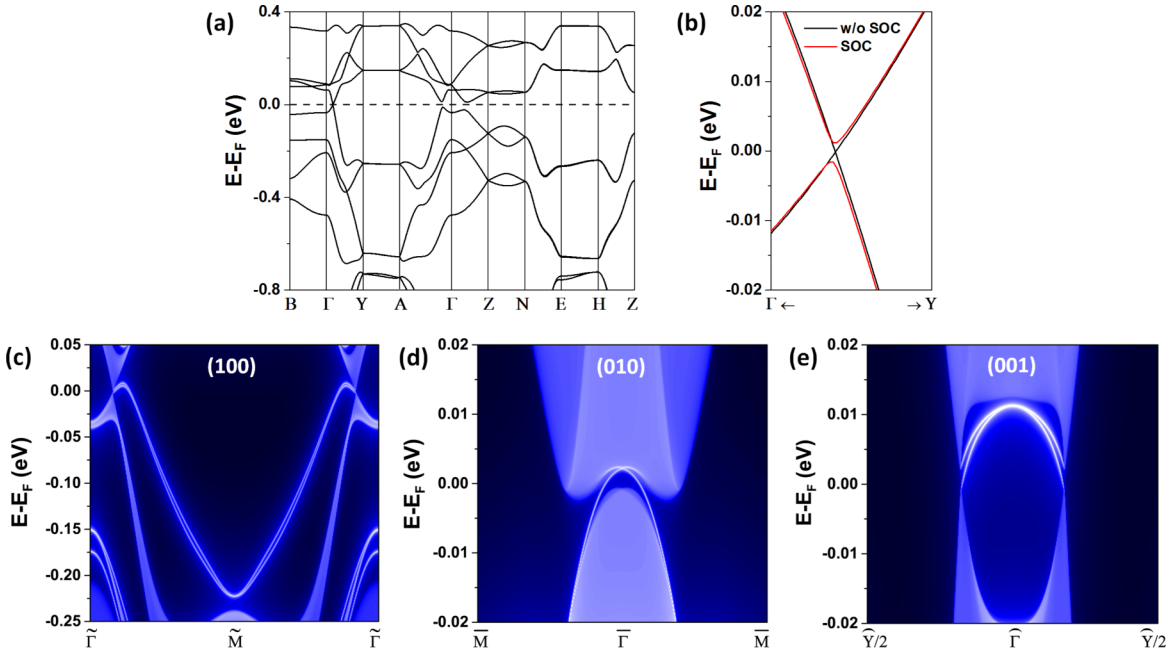

FIG. 5. (a) Band structure of Pd(dddt)$_2$ with SOC at 8 GPa pressure. (b) Zoom-in of band structure around the band degeneracy at Fermi level with and without SOC. (c)–(e) Topological surface state on (100), (010), and (001) surfaces, respectively.

Generally, the SOC can drive the topological nodal-line semimetal into different topological phases. To identify this possibility, the topological invariant (Z_2) of Pd(dddt)$_2$ is calculated. The 3D molecular crystal of Pd(dddt)$_2$ has space inversion symmetry, so that Z_2 index can be easily calculated by accounting the parity at eight time reversal invariant moments (TRIMs) [38]. At N, Z, Y, A four TRIMs, its two generators of the corresponding little group are anticommute with each other. Thus, each band will be fourfold degenerate and includes two Kramers pairs with opposite parity [39,40], labeled as $(+\ -)$. The parity at eight TRIMs for the four occupied bands below the Fermi level is listed in Table II. The corresponding Z_2 index will be (1;000), indicating a strong 3D topological metal phase. As an alternative way to identify the nontrivial topology, the topological surface state can be calculated. Similar to the case without SOC, an eight-band first-principles TB Hamiltonian with SOC is fitted. The corresponding semi-infinite surface state on (100), (010), and (001) surfaces are further calculated. As shown in Figs. 5(c)–5(e), one pair of Dirac surface states, siting at the TRIM, can be seen within the energy window of local SOC gap on all three surfaces. These characteristic signatures further confirm Pd(dddt)$_2$ to be a strong 3D topological metal, consistent with the Z_2 analysis. Quantitatively, however, the SOC gap is very small, a couple of meV, so one expects that the nodal-line properties are still observable experimentally, such as by the magneto-conductivity measurements [41,42].

TABLE II. Parity of occupied bands of Pd(dddt)$_2$.

TRIMs	Parity 1	2	3	4	Product
Γ	−	−	−	+	−
B	+	−	+	−	+
N	(+	−)	(+	−)	+
Z	(+	−)	(+	−)	+
Y	(+	−)	(+	−)	+
A	(+	−)	(+	−)	+
E	+	+	−	−	+
H	+	+	+	+	+
Z_2 index (1;000)					

$(+,-)$ denotes the parity of degenarate two Kramers pairs.

In conclusion, using first-principles calculations, we demonstrate a pressure-induced topological nodal-line semimetal in a recent experimentally synthesized 3D molecular crystal. The SOC further drives the system into a strong 3D topological metal. Our findings not only extend the topological states from 2D to 3D organometallic materials, but also provide a viable platform for searching pressure-induced topological states in 3D molecular crystals with low crystal symmetry. We envision that more 3D organometallic topological materials will be discovered in the future, which will greatly broaden their scientific and technological impacts.

ACKNOWLEDGMENTS

We thank H. Huang for helpful discussions. Z.F.W. is supported by NSFC (Grants No. 11774325 and No. 21603210), National Key Research & Development Program of China (Grant No. 2017YFA0204904), Chinese Youth One Thousand Talents Program and Fundamental Research Funds for the Central Universities. J.L.Y. is supported by NSFC (Grants No. 21233007, No. 21421063, and No. 21603205) and National Key Research & Development Program of China (Grant No. 2016YFA0200604). F.L. is supported by US DOE-BES (Grant No. DE-FG02-04ER46148). We also thank the Supercomputing Center at USTC for providing the computing resources.

[1] Z. Wang, Y. Sun, X.-Q. Chen, C. Franchini, G. Xu, H. Weng, X. Dai, and Z. Fang, Phys. Rev. B **85**, 195320 (2012).

[2] Z. Wang, H. Weng, Q. Wu, X. Dai, and Z. Fang, Phys. Rev. B **88**, 125427 (2013).

[3] Z. K. Liu, B. Zhou, Y. Zhang, Z. J. Wang, H. Weng, D. Prabhakaran, S.-K. Mo, Z. X. Shen, Z. Fang, X. Dai, Z. Hussain, and Y. L. Chen, Science **343**, 864 (2014).

[4] Z. K. Liu, J. Jiang, B. Zhou, Z. J. Wang, Y. Zhang, H. Weng, D. Prabhakaran, S.-K. Mo, H. Peng, P. Dudin, T. Kim, M. Hoesch, Z. Fang, X. Dai, Z. X. Shen, D. L. Feng, Z. Hussain, and Y. L. Chen, Nat. Mater. **13**, 677 (2014).

[5] H. Weng, C. Fang, Z. Fang, B. A. Bernevig, and X. Dai, Phys. Rev. X **5**, 011029 (2015).

[6] S.-M. Huang, S.-Y. Xu, I. Belopolski, C.-C. Lee, G. Chang, B. Wang, N. Alidoust, G. Bian, M. Neupane, C. Zhang, S. Jia, A. Bansil, H. Lin, and M. Z. Hasan, Nat. Commun. **6**, 7373 (2015).

[7] B. Q. Lv, H. M. Weng, B. B. Fu, X. P. Wang, H. Miao, J. Ma, P. Richard, X. C. Huang, L. X. Zhao, G. F. Chen, Z. Fang, X. Dai, T. Qian, and H. Ding, Phys. Rev. X **5**, 031013 (2015).

[8] S.-Y. Xu, I. Belopolski, N. Alidoust, M. Neupane, G. Bian, C. Zhang, R. Sankar, G. Chang, Z. Yuan, C.-C. Lee, S.-M. Huang, H. Zheng, J. Ma, D. S. Sanchez, B. Wang, A. Bansil, F. Chou, P. P. Shibayev, H. Lin, S. Jia, and M. Z. Hasan, Science **349**, 613 (2015).

[9] H. Weng, X. Dai, and Z. Fang, J. Phys.: Condens. Matter **28**, 303001 (2016).

[10] H. Weng, Y. Liang, Q. Xu, R. Yu, Z. Fang, X. Dai, and Y. Kawazoe, Phys. Rev. B **92**, 045108 (2015).

[11] R. Li, H. Ma, X. Cheng, S. Wang, D. Li, Z. Zhang, Y. Li, and X.-Q. Chen, Phys. Rev. Lett. **117**, 096401 (2016).

[12] H. Huang, J. Liu, D. Vanderbilt, and W. Duan, Phys. Rev. B **93**, 201114 (2016).

[13] Y.-H. Chan, C.-K. Chiu, M. Y. Chou, and A. P. Schnyder, Phys. Rev. B **93**, 205132 (2016).

[14] Y. Quan, Z. P. Yin, and W. E. Pickett, Phys. Rev. Lett. **118**, 176402 (2017).

[15] G. Bian, T.-R. Chang, R. Sankar, S.-Y. Xu, H. Zheng, T. Neupert, C.-K. Chiu, S.-M. Huang, G. Chang, I. Belopolski, D. S. Sanchez, M. Neupane, N. Alidoust, C. Liu, B. Wang, C.-C. Lee, H.-T. Jeng, C. Zhang, Z. Yuan, S. Jia, A. Bansil, F. Chou, H. Lin, and M. Z. Hasan, Nat. Commun. **7**, 10556 (2016).

[16] C. Fang, H. Weng, X. Dai, and Z. Fang, Chin. Phys. B **25**, 117106 (2016).

[17] D. Yu, Y. Zhang, and F. Liu, Phys. Rev. B **78**, 245204 (2008).

[18] C. Si, Z. Sun, and F. Liu, Nanoscale **8**, 3207 (2016).

[19] B. Huang, K.-H. Jin, B. Cui, F. Zhai, J. Mei, and F. Liu, Nat. Commun. **8**, 15850 (2017).

[20] L. Zhang, F. Zhai, K.-H. Jin, B. Cui, B. Huang, Z. Zhang, J. Lu, and F. Liu, Nano Lett. **17**, 4359 (2017).

[21] Z. F. Wang, Z. Liu, and F. Liu, Nat. Commun. **4**, 1471 (2013).

[22] Z. F. Wang, Z. Liu, and F. Liu, Phys. Rev. Lett. **110**, 196801 (2013).

[23] Z. F. Wang, N. Su, and F. Liu, Nano Lett. **13**, 2842 (2013).

[24] Z. Liu, Z. F. Wang, J.-W. Mei, Y.-S. Wu, and F. Liu, Phys. Rev. Lett. **110**, 106804 (2013).

[25] Z. F. Wang, K.-H. Jin, and F. Liu, Wiley Interdiscip. Rev. Comput. Mol. Sci. **7**, e1304 (2017).

[26] N. Su, W. Jiang, Z. F. Wang, and F. Liu, Appl. Phys. Lett. **112**, 033301 (2018).

[27] G. Kresse and J. Furthmüller, Comput. Mater. Sci. **6**, 15 (1996).

[28] R. Kato, H. Cui, T. Tsumuraya, T. Miyazaki, and Y. Suzumura, J. Am. Chem. Soc. **139**, 1770 (2017).

[29] A. A. Mostofi, J. R. Yates, Y.-S. Lee, I. Souza, D. Vanderbilt, and N. Marzari, Comput. Phys. Commun. **178**, 685 (2008).

[30] A. A. Soluyanov and D. Vanderbilt, Phys. Rev. B **83**, 235401 (2011).

[31] M. Taherinejad, K. F. Garrity, and D. Vanderbilt, Phys. Rev. B **89**, 115102 (2014).

[32] R. Yu, X.-L. Qi, A. Bernevig, Z. Fang, and X. Dai, Phys. Rev. B **84**, 075119 (2011).

[33] J.-W. Rhim and Y. B. Kim, New J. Phys. **18**, 043010 (2016)

[34] Y. Sun, Y. Zhang, C.-X. Liu, C. Felser, and B. Yan, Phys. Rev. B **95**, 235104 (2017).

[35] K. Mullen, B. Uchoa, and D. T. Glatzhofer, Phys. Rev. Lett. **115**, 026403 (2015).

[36] J. Liu and L. Balents, Phys. Rev. B **95**, 075426 (2017).

[37] C. Fang, Y. Chen, H.-Y. Kee, and L. Fu, Phys. Rev. B **92**, 081201(R) (2015).

[38] L. Fu and C. L. Kane, Phys. Rev. B **76**, 045302 (2007).

[39] Z. Wang, P. Zhang, G. Xu, L. K. Zeng, H. Miao, X. Xu, T. Qian, H. Weng, P. Richard, A. V. Fedorov, H. Ding, X. Dai, and Z. Fang, Phys. Rev. B **92**, 115119 (2015).

[40] X. Wu, S. Qin, Y. Liang, H. Fan, and J. Hu, Phys. Rev. B **93**, 115129 (2016).

[41] R. Singha, A. K. Pariari, B. Satpati, and P. Mandal, Proc. Natl. Acad. Sci. USA **114**, 2468 (2017).

[42] C. Li, C. M. Wang, B. Wan, X. Wan, H.-Z. Lu, and X. C. Xie, Phys. Rev. Lett. **120**, 146602 (2018).